3-15-2018

Age related diffusion and tractography changes in typically developing pediatric cervical and thoracic spinal cord

Mahdi Alizadeh
Thomas Jefferson University

Joshua Fisher
Thomas Jefferson University

Sona Saksena, PhD
Thomas Jefferson University

Yusra Sultan
Drexel University

Chris Conklin, PhD
Thomas Jefferson University

See next page for additional authors

Authors

Mahdi Alizadeh; Joshua Fisher; Sona Saksena, PhD; Yusra Sultan; Chris Conklin, PhD; Devon Middleton; Laura Krisa, PhD; Jürgen Finsterbusch; Adam Flanders; Scott H. Faro; M. J. Mulcahey; and Feroze Mohamed, PhD

NeuroImage: Clinical 18 (2018) 784–792

Contents lists available at ScienceDirect

NeuroImage: Clinical

journal homepage: www.elsevier.com/locate/ynicl

Age related diffusion and tractography changes in typically developing pediatric cervical and thoracic spinal cord

Mahdi Alizadeh[a,b], Joshua Fisher[b], Sona Saksena[b], Yusra Sultan[c], Chris J. Conklin[b], Devon M. Middleton[b], Laura Krisa[d], Jürgen Finsterbusch[e], Adam E. Flanders[b], Scott H. Faro[f], M.J. Mulcahey[d], Feroze B. Mohamed[b,*]

[a] Department of Neurosurgery, Thomas Jefferson University, Philadelphia, PA, United States
[b] Jefferson Integrated Magnetic Resonance Imaging Center, Department of Radiology, Thomas Jefferson University, Philadelphia, PA, United States
[c] Department of Biology, Drexel University, Philadelphia, PA, United States
[d] Department of Occupational Therapy, Thomas Jefferson University, Philadelphia, PA, United States
[e] Department of Systems Neuroscience, University Medical Center Hamburg-Eppendorf, Hamburg, Germany
[f] Department of Radiology, Johns Hopkins University, Baltimore, MD, United States

ARTICLE INFO

Keywords:
Diffusion tensor imaging
Fiber tractography
Age
Pediatric spinal cord

ABSTRACT

Background and objective: Diffusion tensor imaging (DTI) and diffusion tensor tractography (DTT) are two techniques that can measure white matter integrity of the spinal cord. Recently, DTI indices have been shown to change with age. The purpose of this study is (a) to evaluate the maturational states of the entire pediatric spinal cord using DTI and DTT indices including fractional anisotropy (FA), mean diffusivity (MD), mean length of white matter fiber tracts and tract density and (b) to analyze the DTI and DTT parameters along the entire spinal cord as a function of spinal cord levels and age.

Method: A total of 23 typically developing (TD) pediatric subjects ranging in age from 6 to 16 years old (11.94 ± 3.26 (mean ± standard deviation), 13 females and 10 males) were recruited, and scanned using 3.0 T MR scanner. Reduced FOV diffusion tensor images were acquired axially in the same anatomical location prescribed for the T2-weighted images to cover the entire spinal cord (C1-mid L1 levels). To mitigate motion induced artifacts, diffusion directional images were aligned with the reference image (b0) using a rigid body registration algorithm performed by in-house software developed in Matlab (MathWorks, Natick, Massachusetts). Diffusion tensor maps (FA and MD) and streamline deterministic tractography were then generated from the motion corrected DTI dataset. DTI and DTT parameters were calculated by using ROIs drawn to encapsulate the whole cord along the entire spinal cord by an independent board certified neuroradiologist. These indices then were compared between two age groups (age group A = 6–11 years (n = 11) and age group B = 12–16 years (n = 12)) based on similar standards and age definitions used for reporting spinal cord injury in the pediatric population. Standard least squared linear regression based on a restricted maximum likelihood (REML) method was used to evaluate the relationship between age and DTI and DTT parameters.

Results: An increase in FA (group A = 0.42 ± 0.097, group B = 0.49 ± 0.116), white matter tract density (group A = 368.01 ± 236.88, group B = 440.13 ± 245.24) and mean length of fiber tracts (group A = 48.16 ± 20.48 mm, group B = 60.28 ± 23.87 mm) and a decrease in MD (group A = 1.06 ± 0.23 × 10^{-3} mm^2/s, group B = 0.82 ± 0.24 × 10^{-3} mm^2/s) were observed with age along the entire spinal cord. Statistically significant increases have been shown in FA (p = 0.004, R^2 = 0.57), tract density (p = 0.0004, R^2 = 0.58), mean length of fiber tracts (p < 0.001, R^2 = 0.5) and a significant decrease has been shown in MD (p = 0.002, R^2 = 0.59) between group A and group B. Also, it has been shown DTI and DTT parameters vary along the spinal cord as a function of intervertebral disk and mid-vertebral body level.

Conclusion: This study provides an initial understanding of age related changes of DTI values as well as DTT metrics of the spinal cord. The results show significant differences in DTI and DTT parameters which may result from decreasing water content, myelination of fiber tracts, and the thickening diameter of fiber tracts during the

* Corresponding author at: 909 Walnut Street, Jefferson Integrated Magnetic Resonance Imaging Center, Department of Radiology, Thomas Jefferson University, Philadelphia, PA 19107, United States.
E-mail address: feroze.mohamed@jefferson.edu (F.B. Mohamed).

https://doi.org/10.1016/j.nicl.2018.03.014
Received 24 May 2017; Received in revised form 2 March 2018; Accepted 14 March 2018
Available online 15 March 2018

maturation process. Consequently, when quantitative DTI and DTT of the spinal cord is undertaken in the pediatric population an age and level matched normative dataset should be used to accurately interpret the quantitative results.

1. Introduction

Conventional diagnostic techniques such as magnetic resonance imaging (MRI) have been used to demonstrate significant microstructural changes of neural tissue during the development and maturation of children through their adolescence. Reports have shown that through childhood and adolescence there is a global increase in brain white matter (WM) density as well as a decline in gray matter density (Giedd et al., 1999; Giorgio et al., 2010; Giorgio et al., 2008). In recent years, techniques like diffusion tensor imaging (DTI), a powerful quantitative tool used to measure the diffusivity of water molecules in tissue (Mulcahey et al., 2013; Beaulieu, 2002; Maier and Mamata, 2005; Stiles and Jernigan, 2010; Hüppi and Dubois, 2006) as well as diffusion tensor tractography (DTT) (Kanehiro et al., 2013), a visual and quantitative whiter matter fiber tracking technique, have been used to investigate these changes. These increases/decreases in tissue density have been found to strongly correlate to age-related increases/decreases in DTI and DTT metrics (Hüppi and Dubois, 2006; Kanehiro et al., 2013; Izbudak et al., 2015; Singhi et al., 2012); fractional anisotropy (FA), apparent diffusion coefficient (MD), tract density and length of fiber tracts (average Euclidean length in mm for all streamlines within a given segment) in the brain. These findings are highly supportive of the hypothesis that age-related maturation and development continue through to adulthood.

DTI and DTT have been used in past studies to investigate the WM and its axonal projections in the brain. Reports have shown the reliability of DTI and DTT in the analysis of pediatric epilepsy (Helen et al., 2014), severity of WM damage in the brain following stroke (Iannetti et al., 2011), and the maturation of brain white matter tracts through typical development (Cancelliere et al., 2013). However, to the best of our knowledge, little has been reported on the white matter changes that occur in the spinal cord, especially with pediatric subjects. This is a result of the smaller size of the spinal cord compared to the brain and the challenges associate with diffusion imaging of the cord. Presence of anatomical structures such as muscle and bone that are in close proximity to the spinal cord increase image artifacts due to susceptibility changes (Barakat et al., 2012). Furthermore, image degradation can occur as a result of physiological and patient motion. Typically, gating strategies are used to mitigate motion effects from patient movement, CSF pulsation, cardiac, and respiratory cycles. These gating techniques increase acquisition time, which poses a problem when scanning children (Iannetti et al., 2011; Cancelliere et al., 2013; Barakat et al., 2012). In pediatric cases, these problems are more pronounced due to the smaller overall size of the cord compared to adults. In the last several years, development of new pulse sequences like reduced field of view (FOV) have now proven to be achievable and reliably acquired further reducing the effect of physiologic motion while increasing in-plane resolution (Barakat et al., 2012; Saksena et al., 2016).

A few recent studies have used DTI to investigate diffusion in the pediatric spinal cord. These studies have characterized normal diffusion metrics in typically developing (TD) subjects (Barakat et al., 2012; Saksena et al., 2016; Mohamed et al., 2011; Figley and Stroman, 2007). Other studies have used DTI and DTT to compare pediatric spinal cord injuries (SCI) with TD subjects (Chang et al., 2010; Alizadeh et al., 2017). A major shortcoming of these research explorations is the failure to consider natural variation of DTI and DTT metrics as a result of aging and maturation. One study, in particular, reported DTI indices of FA and MD values in subjects ranging from infancy through adolescence (Cancelliere et al., 2013). However, to our knowledge, there have been no investigations of age related diffusion and tractography changes in the entire spinal cord of the TD population. In this study, DTI and DTT were utilized to investigate age-related diffusion and tractography changes in the typically developing pediatric cervical and thoracic spinal cord. These techniques show potential as sensitive and effective measures of the microstructural changes of the spinal cord that transpire during maturation.

2. Methods

2.1. Subject recruitment

A total of 23 TD pediatric subjects with ages ranging from 6 to 16 years old (11.94 ± 3.26 (mean ± standard deviation), 13 females and 10 males) with no evidence of spinal cord injury or pathology were recruited for this study. Subjects and parents provided written assent and consent of the institutional review board approved protocol. Subjects were divided into two age groups, group A = 6–11 years old (n = 11) and group B = 12–16 years old (n = 12) based on similar standards and age definitions used for reporting spinal cord injury in the pediatric population (Saksena et al., 2016; DeVivo and Vogel, 2004).

2.2. Image acquisition

Subjects were scanned in a 3.0 T Siemens Verio MR scanner (Siemens Healthcare, Erlangen, Germany) using a 4-channel neck matrix and 8-channel spine matrix coils.

The protocol consisted of a conventional sagittal turbo spin echo (TSE)-T1-weighted scan, a sagittal TSE-T2-weighted scan, axial T2-weighted gradient echo (GRE). DTI scans based on a 2D radiofrequency (RF) reduced field of view (rFOV) pulse sequence using a tilted excitation plane were collected axially in the same anatomical location prescribed for the T2-weighted images to cover the entire spinal cord (C1 to mid-L1 levels) using two overlapping slabs. The excitation plane was tilted to allow for shorter 2DRF pulses and ensure that the sidelobes are not present in the refocusing plane. This ensures that the excitation does not interfere with the current, as well as, subsequent slices measured. In each slab 40 individual axial slices were acquired. The first slab was prescribed to collect images from superior C1 to mid thoracic. The second slab covered mid thoracic to the mid-L1 disc level (with one to two levels of overlap with slab one).

The rFOV sequence was based on a double refocused echo-planar imaging (EPI) sequence with 2D-selective radiofrequency (RF) excitations which allows for a higher in-plane resolution while minimizing distortion as a result of the shorter phase-encoding readout in the AP direction (Finsterbusch, 2012). Manual shim and fat saturation volume adjustments were also performed before data acquisition to confine the adjustment volume to the anatomy of interest as much as possible to limit residual distortions and chemical-shift artifacts.

The T2-weighted GRE imaging parameters used were: voxel size = 0.42 × 0.42 × 6.0 mm^3, matrix size = 384 × 384, TR = 878 ms, TE = 8 ms, slice thickness = 6 mm, flip angle = 25°, number of averages = 1 and acquisition time = 2.17 min (each overlapping slab). The DTI parameters used were: FOV = 164 mm, phase FOV = 28.4% (47 mm), number of directions = 20, b = 800 s/mm^2, voxel size = 0.8 × 0.8 × 6.0mm^3, matrix size = 36 × 208, axial slices for each slab = 40, TR = 7900 ms, TE = 110 ms, number of averages = 3, slice thickness = 6.0 mm, slice gap = 0, number of b0 volumes = 6 and acquisition time = 8.82 min (to collect each slab).

In order to keep the acquisition time to a minimum neither gating nor anesthesia were used during scanning.

3. Pre-processing of data

3.1. Motion correction

While the implementation of the 2DRF diffusion sequence helped to mitigate image contamination due to patient movement, and some cardiac and respiratory motion within the cervical cord, motion correction was performed to further enhance tensor estimation accuracy (Middleton et al., 2014). The diffusion data sets were corrected for motion induced artifacts based on 3D registration technique using an in-house software developed in Matlab (MathWorks, Natick, Massachusetts) (Saksena et al., 2016; Middleton et al., 2014). The technique uses rigid body transformation with 6 degrees of freedom (3 translational, 3 axis rotations) paired with normalized mutual information as cost function to align target images (20 diffusion directional images) with the reference image (b0).

3.2. Diffusion tensor estimation

Using the preprocessed data, DTI maps such as FA and MD were produced using robust estimation of tensor by outlier rejection (RESTORE). This RESTORE technique takes the reweighted least-squares regression to determine and exclude any existing signal outliers caused by physiologically generated artifacts (Chang et al., 2005).

4. Generation of fiber tracts

Following DTI image acquisition and pre-processing of the data, DTT images were generated using the deterministic fiber tracking approach (Fig. 1 and Fig. 2). Neural fiber seed and termination points were defined using the DTI estimated FA parameter map as a threshold value to incorporate regions of high diffusion directionality (WM). The FA threshold was set to 40–50% below the averaged FA value (0.18–023) across all subjects. Fiber assignments of deterministic tractography was performed at each of the seed points (voxel) belonging to the WM (with FA greater than the pre-defined threshold) of every slice to generate whole spinal cord tracts followed by propagation along the dominant diffusion orientation by setting the length and step size of the fiber trajectories. A tract is terminated when it reaches a voxel with FA values lower than the predefined threshold (0.18–0.23) as well as an angular constraint for turning fiber orientation (i.e., 70°) (Alizadeh et al., 2017; Knosche et al., 2015). These tracts were then restricted to the user defined ROIs placed at each intervertebral disk level and at the mid-vertebral body level of the cervical and thoracic spinal cord (approximately 40 ROIs).

5. ROI definition

Region of interests (ROIs) were drawn manually on each FA map at each intervertebral disk level and at the mid-vertebral body level of the cervical and thoracic spinal cord to compute DTI and DTT measures. These ROIs were anatomically localized by an independent board certified neuroradiologist, per subjects using sagittal turbo spin echo (TSE)-T1-weighted scan localized with axial T2-wighted GRE images. Fig. 3 provides an example of ROIs for several positions along the spinal cord.

Manual ROIs were drawn around the gray and white matter of the cord in the FA map. To avoid any partial volume artifacts which occur at the cord/CSF interface, the ROI borders were drawn approximately 1–2 voxels away from the perimeter of the spinal cord (Conklin et al., 2016). The following levels were included: C1, mid-dens, base dens, mid-C2, C2–C3, mid-C3 (upper cervical cord); C3–C4, mid-C4, C4–C5, mid-C5 (middle cervical cord); C5–C6, mid-C6, C6–C7, mid-C7, C7–T1 (lower cervical cord); mid-T1, T1–T2, mid-T2, T2–T3, mid-T3, T3–T4, mid-T4, T4–T5 (upper thoracic cord); mid-T5, T5–T6, mid-T6, T6–T7, mid-T7, T7–T8, mid-T8, T8–T9 (middle thoracic cord); mid-T9, T9–T10, mid-T10, T10–T11, mid-T11, T11–T12, mid-T12, T12–L1, mid-L1 (lower thoracic cord).

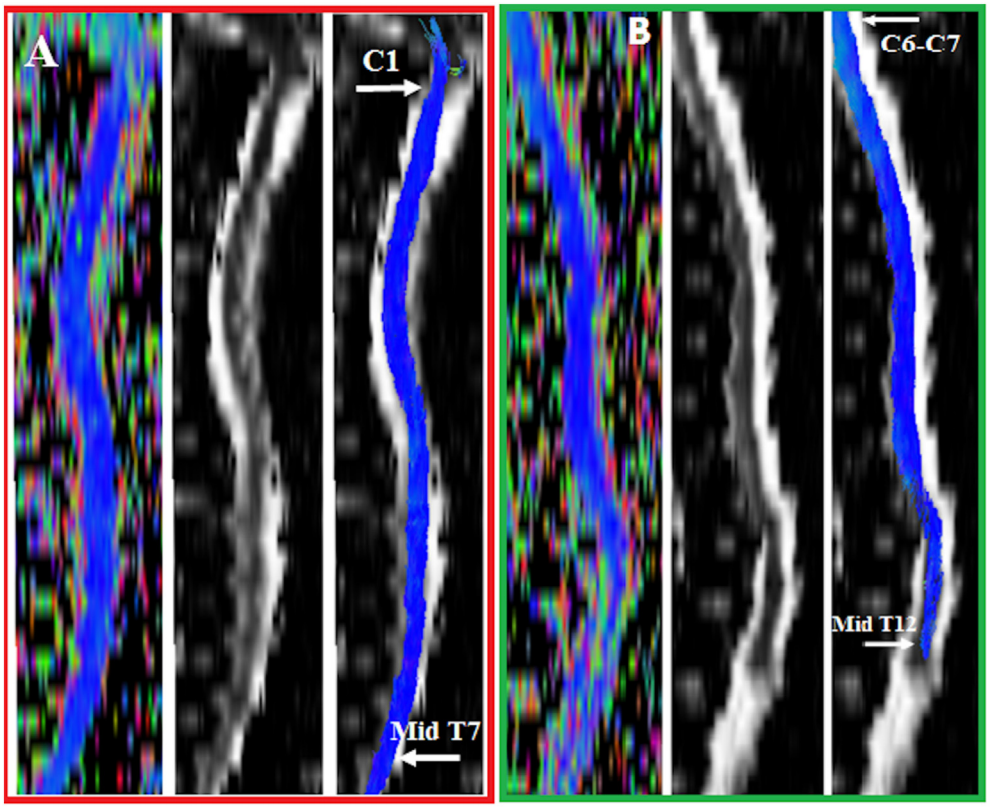

Fig. 1. Sagittal reconstruction of FA color maps and MD maps of 2 overlapping slabs (A and B). The cervical and middle thoracic regions (A): FA color map (left), MD (middle) and tractography (right). The lower cervical through lower thoracic (B): FA color map (left), MD (middle) and tractography (left). (For interpretation of the references to color in this figure legend, the reader is referred to the web version of this article.)

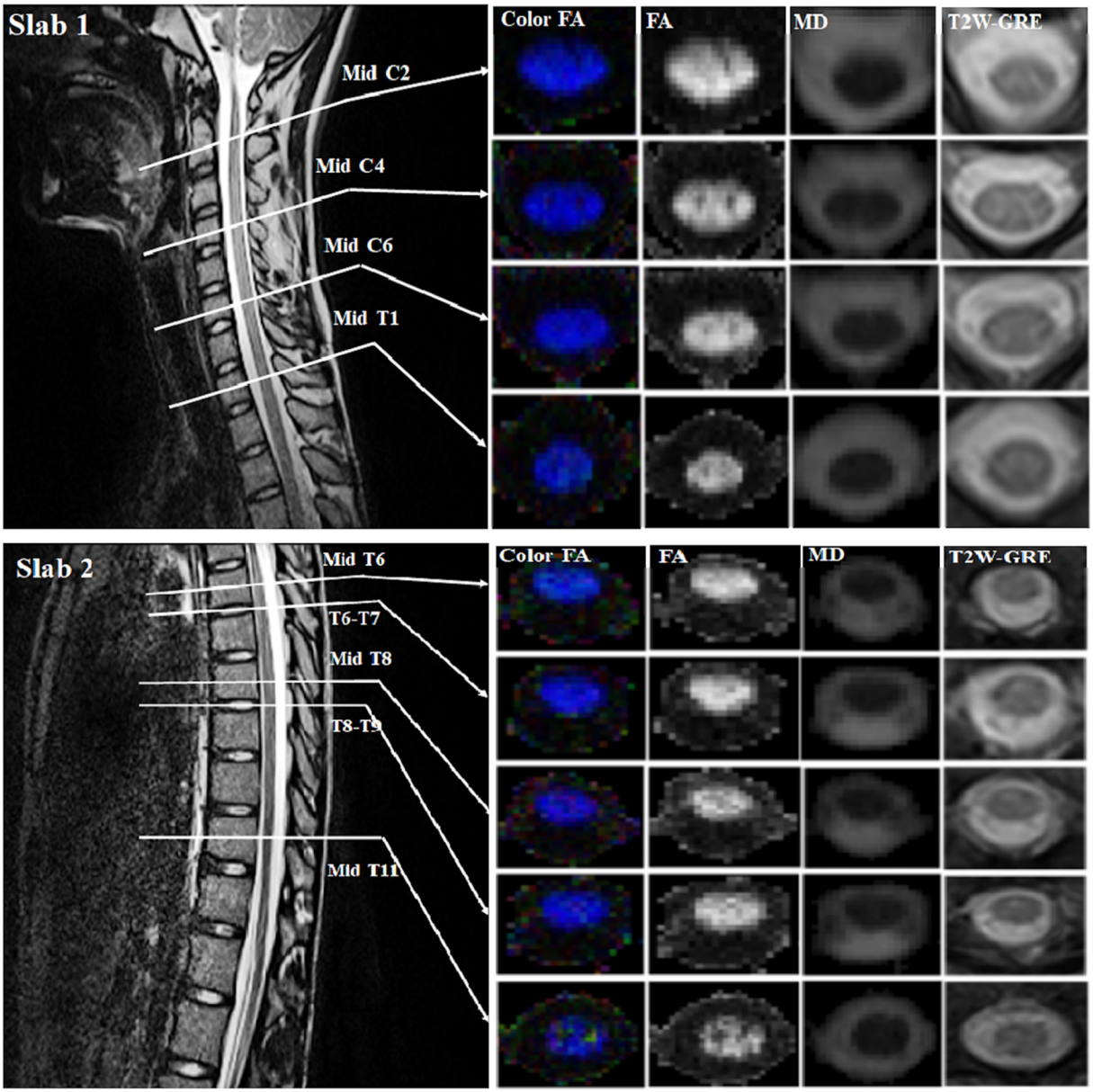

Fig. 2. Axial color FA, FA, MD and T2W-GRE images for a single subject at different spinal cord levels.

5.1. Statistics

Intra-age group and inter-age group statistics were performed at the levels defined in Section VI. The mean and standard deviation of each DTI and DTT measure, including FA, MD, tract density, and length of tracts for every subject along the entire spinal cord at each inter-vertebral disk level and at the mid-vertebral body level of the cervical and thoracic spinal cord were calculated (Table 1). These indices then were compared between two age groups (age group A = 6–11 years (n = 11) and age group B = 12–16 years (n = 12)) based on standard least squared linear regression model and the restricted maximum likelihood (REML) method.

This model was constructed looking at group differences by assuming ROI level and groups (controls/patients) composition as the fixed effects and subjects as the random effects.

The REML methodology performs maximum likelihood estimation of a restricted likelihood function that does not depend on the fixed-effect parameters. This yields estimates of the variance components that are then used to obtain the estimates of the fixed effects. Estimates of precision are based on estimates of the covariance matrix which modeled as unstructured and repeated based on level. It provides useful estimates, tests, and confidence intervals. To determine statistical significance, a P value of 0.05 was used throughout (Chang et al., 2010).

DTI and DTT parameters were compared between age groups as a function of cord levels (intervertebral disk levels and mid-vertebral body levels) (Fig. 4) and age (Fig. 5). Additionally, eight specific spinal cord regions were defined: cervical, thoracic, upper-cervical (CUP), mid-cervical (CMID), lower-cervical (CLOW), upper-thoracic (TUP), mid-thoracic (TMID), and lower-thoracic (TLOW). The mean values among the upper, middle, and lower cervical and thoracic spinal cord were calculated and corresponding regions were compared between age groups (Table 2).

6. Results

The mean FA values for subjects in group A were 0.42 ± 0.097 while group B produced a mean FA of 0.49 ± 0.116. Statistics revealed that there was a significant increase in FA in the more mature group B

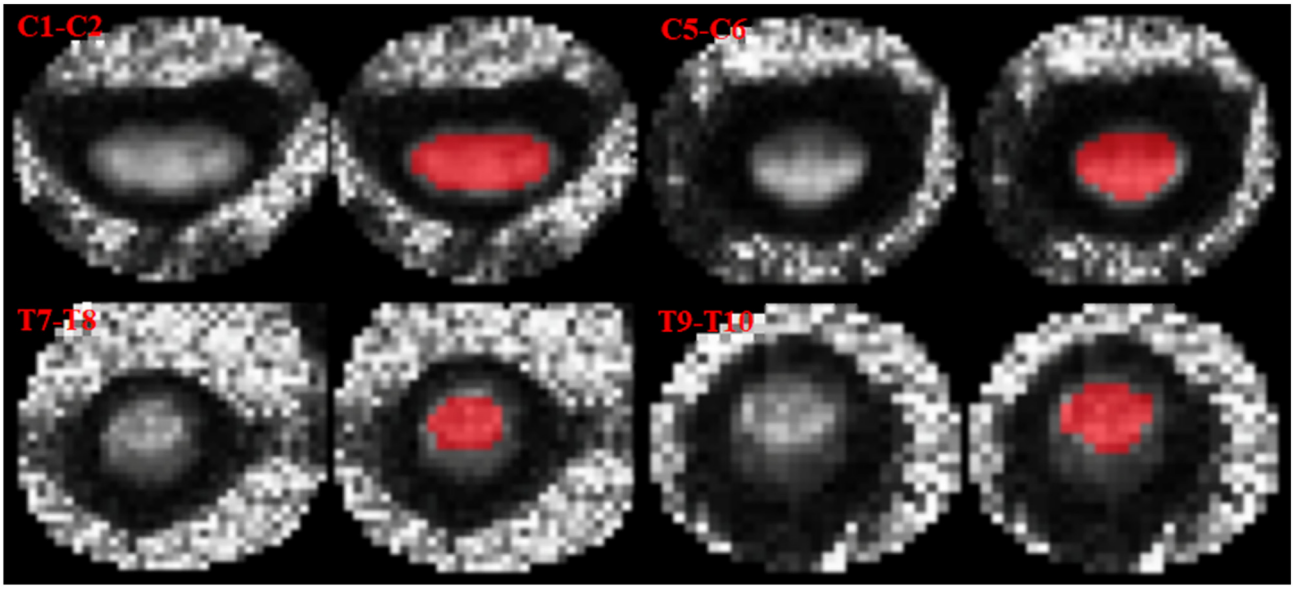

Fig. 3. An example of ROIs for several positions along the spinal cord.

($p = p = 0.004$, $R^2 = 0.57$) compared to the younger group A. The same was true for white matter tract density and mean length of fiber tracts. Tract density significantly increased ($p = 0.0004$, $R^2 = 0.58$) in group B (440.13 ± 245.24) compared to group A (368.01 ± 236.88). Mean length of fiber tracts significantly increased ($p < 0.001$, $R^2 = 0.5$) in group B (61.56 ± 35.65 mm) compared to group A (48.16 ± 20.48 mm). MD was the only parameter to show a significant decrease ($p = 0.002$, $R^2 = 0.59$). The older group B had an MD = $1.06 \pm 0.23 \times 10^{-3}\,mm^2/s$ while group A's MD = $0.82 \pm 0.24 \times 10^{-3}\,mm^2/s$.

Additionally, average DTI and DTT parameters of each age group were plotted as a function of individual cord levels. Fig. 4 shows a significant increase in mean FA, tract density, and mean length of tract of group B compared to group A. Also, there was a significant decrease in mean MD of group B compared to group A.

Next, DTI and DTT parameters were plotted against age using a simple linear regression analysis. As seen in Fig. 5, there was an increase in FA, tract density, and length of tract while MD decreased as age increased. Also, the size of ROIs as a function of cord levels were plotted in Fig. 6. The Pearson correlation coefficient were used to correlate DTI and DTT measures with size of cord. The results reveal strong correlation between spinal cord size and DTI and DTT indices (FA [$r = 0.99$], MD [$r = -0.7$], tract density [$r = 0.98$] and length of tract [$r = 0.55$]).

To study the changes in DTI and DTT parameters among different levels of the cervical and thoracic spinal cord, we averaged DTI and DTT values across the following regions per subject: CUP, CMID, CLOW, TUP, TMID and TLOW. The mean values were used for comparison among the upper, middle, and lower cervical and thoracic spinal cord across all subjects. Table 2 shows the *p*-value for each subregion. The significant values are shown in bold.

7. Discussion

Previous studies in adult's cervical spinal cord DTI have been shown decrease in FA and increase in MD as a function of age (Chan et al., 2015; Vedantam et al., 2013; Wang et al., 2014) while in pediatric, FA increases and MD decrease. The observed increase in mean FA may be a result of increased diameter of the fiber tracts following the increase in axonal membranes and myelin density during the process of maturation. The decrease in MD is likely tied to the decrease in extracellular space and water content (Saksena et al., 2016). To the best of our knowledge, this is first study looking for age related DTI and DTT changes along cervical and thoracic spinal cord. The older group B, ages 12–16, revealed a significant increase in mean FA and decrease in mean MD compared to the younger group A, ages 6–11. As an extension of the brain, the spinal cord is likely to undergo similar maturational processes. The observed increase in mean FA may be a result of increased diameter of the fiber tracts following the increase in axonal membranes and myelin density. The decrease in mean MD is likely tied to the decrease in extracellular space and water content (Saksena et al., 2016). Previous studies in brain shows myelination is a major contributor and is likely accompanied by increased axonal packing and decreasing water content (Lebel and Deoni, 2018).

To gain further quantitative and empirical insight, DTT has become a supplementary tool to DTI. Along with DTI parameters FA and MD, DTT produces informing measures such as tract density and length of fiber tracts. Few reports on the use of fiber tracking in the typically developing pediatric spinal cord have been published. Most studies that have been done have used healthy pediatric controls as comparisons to abnormal spinal cord conditions. For example, fiber tracking has been used to investigate the inflammatory cord in patients with myelitis (Renoux et al., 2006), as a predictor of the resectability of spinal cord

Table 1
DTI and DTT measures for each age group.

	Group A (Ages 6–11) $n = 11$ Mean ± Std	Group B (Ages 12–16) $n = 12$ Mean ± Std	Prob > |t|
FA	0.42 ± 0.097	0.49 ± 0.116	$p = 0.016$
MD ($10^{-3}\,mm^2/s$)	1.06 ± 0.23	0.82 ± 0.24	$p = 0.0078$
Tract density	368.01 ± 236.88	440.13 ± 245.24	$p < 0.0001$
Length of tracts (mm)	48.16 ± 20.48	60.28 ± 23.87	p = 0.0004

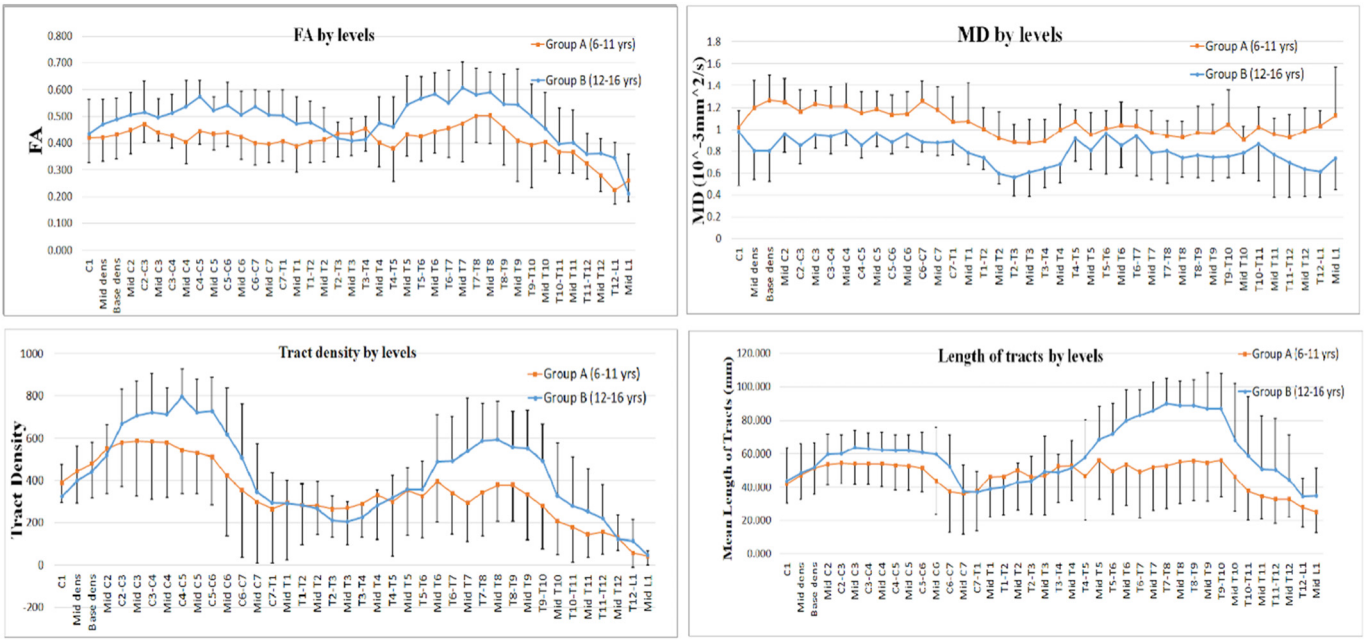

Fig. 4. DTI and DTT parameters averaged across all the controls per age groups and plotted as a function of cord levels. The error bars represent the standard deviation.

tumors (Setzer et al., 2010), and the severity of spinal cord injuries (Chang et al., 2010; Alizadeh et al., 2017; Facon et al., 2005). In all these cases, healthy pediatrics were used as a comparison to the abnormal patients. A major shortcoming of these studies is the failure to consider natural age related variation in control groups. What is considered typically developing in an eight year old child may not be considered healthy for an adolescent. To test for this natural variation, length of fiber tracts and tract density were calculated by use of deterministic fiber tracking. Analysis of the data revealed significant increases in both tract density and length of tracts.

Significant increases and decreases in both DTI and DTT metrics is a clear indicator of biological development from childhood through adolescence. Giedd et al. conducted a study on 145 subjects ranging from ages 4–20 years. They found a steady 12% significant increase in brain white matter volume as the subjects age (Giedd et al., 1999). Paus et al found that in the cortico-spinal tract and left arcuate fasciculus, white matter volume significantly increases between ages 4 and 17 (Paus, 2010). Another relevant study looked at the age-related changes in axonal diameter from childhood to adulthood. They observed that the largest axons of the brain, located in the internal capsule, increase

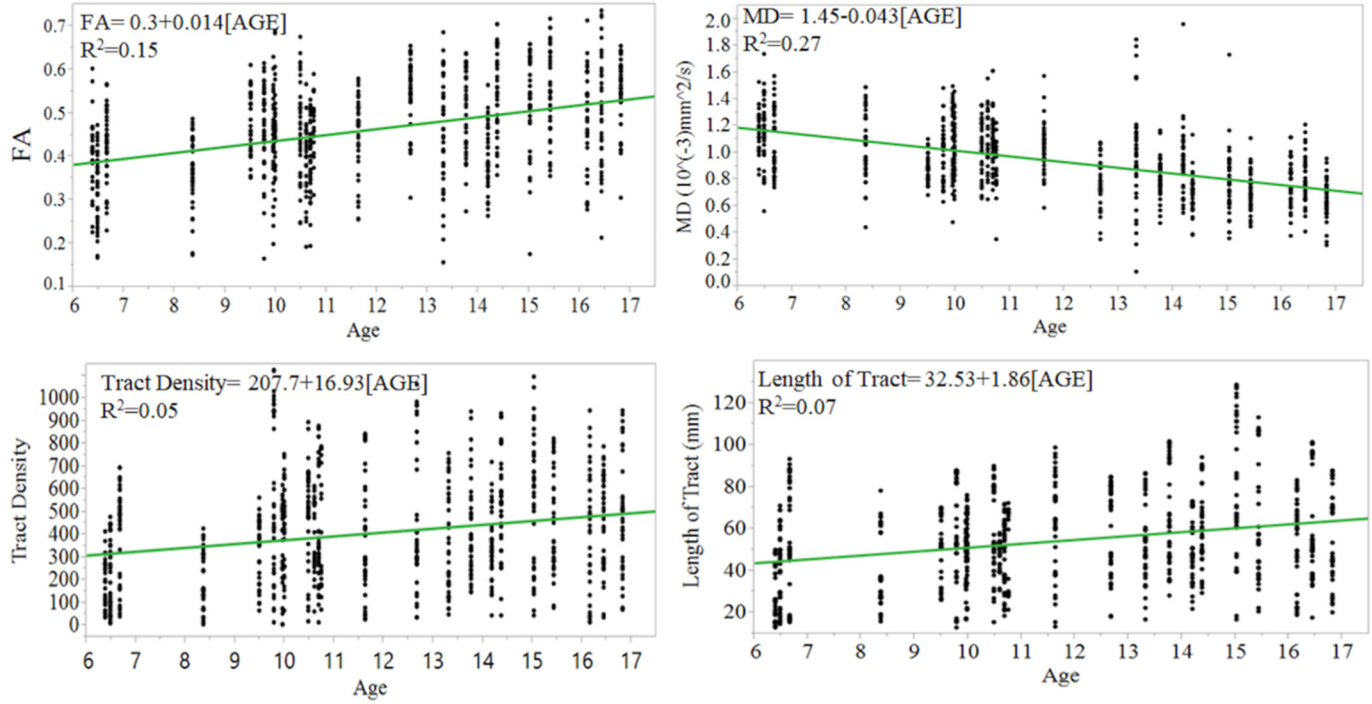

Fig. 5. Linear fit plots showing the relationship of FA, MD, Tract Density, and Length of Tract as a function of age in typically developing pediatric subjects. Each point represents the whole cord DTI/DTT measures at each axial slice corresponding to the intervertebral disk level and at axial slice corresponding to the mid-vertebral body level of the cervical and thoracic spinal cord (approximately 40 slices per subject).

Table 2
the p-value calculated for regional DTI and DTT parameters.

Value		
FA	$Cervical_A$ vs $Cervical_B$: $P = 0.15$	**$Thoracic_A$ vs $Thoracic_B$: P < 0.001**
	CUP_A vs CUP_B: $P = 0.97$	$CMID_A$ vs $CMID_B$: $P = 0.29$
	$CLOW_A$ vs $CLOW_B$: $P = 0.77$	**TUP_A vs TUP_B: P = 0.002**
	$TMID_A$ vs $TMID_B$: $P = 0.46$	$TLOW_A$ vs $TLOW_B$: $P = 0.19$
MD	**$Cervical_A$ vs $Cervical_B$: P = 0.004**	**$Thoracic_A$ vs $Thoracic_B$: P = 0.034**
	CUP_A vs CUP_B: P = 0.01	$CMID_A$ vs $CMID_B$: $P = 0.17$
	$CLOW_A$ vs $CLOW_B$: P = 0.01	TUP_A vs TUP_B: $P = 0.31$
	$TMID_A$ vs $TMID_B$: $P = 0.78$	**$TLOW_A$ vs $TLOW_B$: P = 0.03.**
Tract Density	**$Cervical_A$ vs $Cervical_B$: P = 0.008**	**$Thoracic_A$ vs $Thoracic_B$: P < 0.001**
	CUP_A vs CUP_B: $P = 0.18$	$CMID_A$ vs $CMID_B$: P = 0.17
	$CLOW_A$ vs $CLOW_B$: P = 0.05	TUP_A vs TUP_B: $P = 0.85$
	$TMID_A$ vs $TMID_B$: P < 0.001	$TLOW_A$ vs $TLOW_B$: $P = 0.52$.
Length of Tract	$Cervical_A$ vs $Cervical_B$: $P = 0.43$	**$Thoracic_A$ vs $Thoracic_B$: P < 0.001**
	CUP_A vs CUP_B: $P = 0.89$	$CMID_A$ vs $CMID_B$: $P = 0.53$
	$CLOW_A$ vs $CLOW_B$: P = 0.01	TUP_A vs TUP_B: $P = 0.14$
	$TMID_A$ vs $TMID_B$: P = 0.002	$TLOW_A$ vs $TLOW_B$: $P = 0.89$.

from 1 μm at birth, to 12 μm at age 7 and finally up to 24 μm in adulthood. This increase in axonal diameter corresponds to the increase axonal caliber and myelin sheath. As part of the CNS, we can hypothesize that these biological changes occur in the spinal cord as well (Lassek, 1942; Verhaart, 1950). Therefore, in the older aged group B of our study, the significant increases in FA, tract density, length of tracts and decrease in MD is likely a cause of an increase in white matter volume and axon diameter.

Mean DTI and DTT values calculated from whole cord analysis provided important insight into diffusion along the entire spinal cord. However, it is well documented that different vertebral levels and regions have unique structural differences from each other. One study found that the spinal cord has two enlargements at the cervical and lumbar levels. This is due to the higher density of neural tissue that the brachial and lumbar plexuses require (Sherman et al., 1990). The smallest diameter can be found in the thoracic region, specifically T7 (Ko et al., 2004). To investigate these regional differences, the cervical and thoracic spinal cord were each split into upper, middle, and lower categories for each age group. In doing so, a number of significant increases or decreases were observed. Statistical analysis revealed fourteen significant differences between the two age groups.

Upon analysis, DTI measurements showed significant increases of FA in the thoracic and upper thoracic regions as well as significant decreases in MD in cervical, thoracic, upper cervical, lower cervical and lower thoracic stratifications. It has been demonstrated that the ratio of gray matter to total transverse area is 18% in the cervical cord compared to 13.2% in the thoracic while lumbar cord is the greatest at 36.3% (Goto and Otsuka, 1997). To supplement this, reports have shown that there is a linear decrease in gray matter as a subject ages (Good et al., 2001). Therefore, it is plausible to see an increase in FA in the thoracic regions where there is decreased gray matter, an inherently isotropic tissue. The decrease of MD in the older group B is likely a factor of the natural enlargement of the cervical and lumbar spinal cord, due to increased density of myelin and axonal membranes and thus restriction of diffusion.

Regional analysis of DTT metrics showed significant increases in tract density and length of the tract of the thoracic, lower cervical and mid thoracic levels. Tract density additionally showed an increase when comparing the cervical spinal cord between the two groups. One study, looking at postnatal changes of segment length in spinal cord segments showed that from newborn to adult, there is a 2.7 times increase in whole cord length, with the thoracic region showing greatest increase at 304% followed by 238% increase for both the cervical and lumbar spinal cord (Lassek and Rasmussen, 1938). As a result, the increase in both tract density and length during the maturational period are due to these natural growth increases.

The small size of the pediatric spinal cord was a major limitation for this pediatric imaging study. Even when imaging adult subjects, it is difficult to separate the white and gray matter in the spinal cord with the spatial resolution that is achievable. To analyze the data, ROIs were manually drawn to separate tissue from CSF. Manual ROI definition is a very inefficient and time consuming process that does not allow for the segmentation of GM from WM. Therefore, the DTI and DTT metrics that were calculated were the average GM and WM diffusion characteristics. This obstacle could be solved with an automated or semi-automated segmentation method that accurately delineates WM and GM across cervical and thoracic spinal cord.

However, GM segmentation is challenging due to small cross-

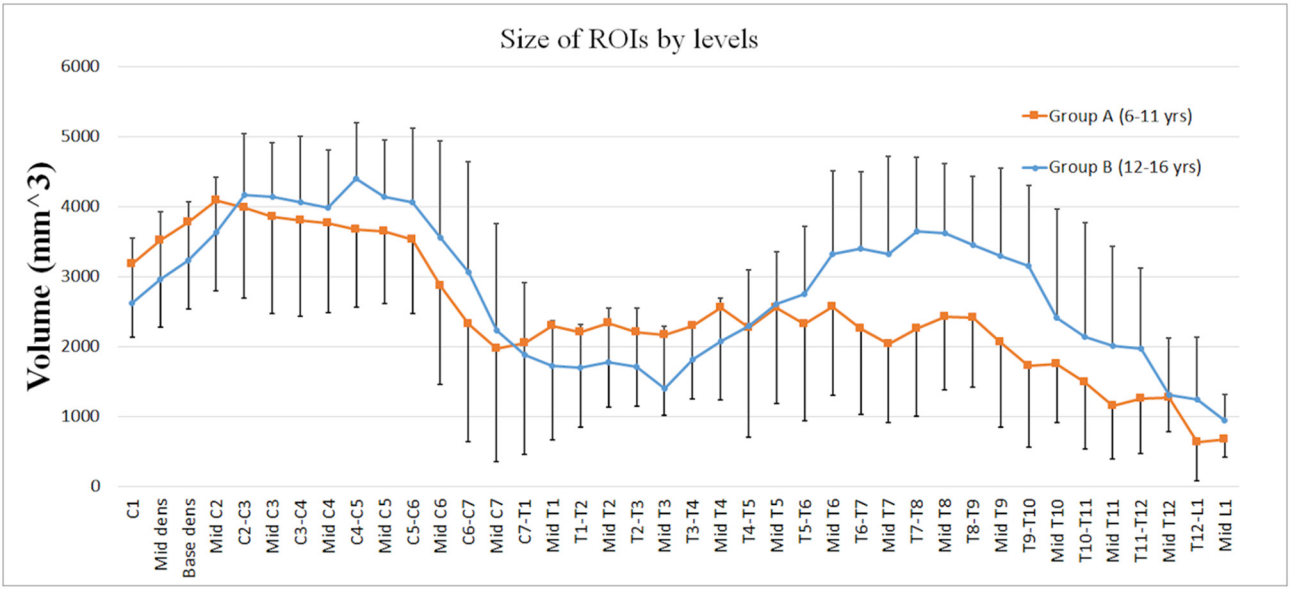

Fig. 6. Size of ROIs manually drown at each intervertebral disk levels and mid-vertebral body levels. The error bars represent the standard deviation.

sectional size and shape, and active research is being conducted by several groups around the world in this field (Prados et al., 2017). Currently, no automatic methods exist for delineating WM and GM from DTI spinal cord images along cervical and thoracic spinal cord in pediatric. Therefore, in future, an automated or semi-automated segmentation method is required for accurately delineating the GM and WM in the spinal cord. There is also the need to acquire high resolution DTI at a higher field strength, with improved radiofrequency coils and multiband DTI techniques, which will allow imaging small voxels while still maintaining a relatively short imaging time.

The fiber tracts of the cord were generated using a deterministic streamline approach. This method has proven to be an effective algorithm capable of estimating the trajectories of white matter tracts in the brain and the cord (Chang et al., 2010; Alizadeh et al., 2017; Mori and Van Zijl, 2002). However, deterministic fiber tracking has limitations, particularly in voxels where fibers are crossing, bending or kissing. The spinal cord has various ascending and descending tracts in close proximity to each other that turn and cross at different levels. With a voxel size of $0.8 \times 0.8 \times 6.0$ mm, it is possible that a voxel will contain fibers of different orientations. The origin of this crossing fibers problem lies in the fact that DTI requires a relatively low number of diffusion weighted directions, causing the tract to terminate or be generated inaccurately. One way to resolve this problem is to use other diffusion imaging techniques that use a higher number of gradient directions such as High Angular Resolution Diffusion Imaging (HARDI) or Neurite Orientation Dispersion and Density Imaging (NODDI) (Zhang et al., 2012; Berman et al., 2013) in conjunction with probabilistic fiber tracking. Probabilistic fiber tracking evaluates all possible propagation directions to generate the neural tracts. With more gradient directions and therefore a higher angular resolution, more accurate production of fibers is possible. However, diffusion weighted images with such high b-value have low SNR but due to the increased contrast-to-noise ratio in the angular domain they provide better delineation of crossing fibers (Tournier et al., 2012). Previous studies in the brain suggest that the optimal b-value to use for estimation of fiber orientations in crossing fiber voxel is ~2500–3000 s/mm^2, although good results can still obtain using lower b-value (~1000 s/mm^2) (Tournier et al., 2012; Tournier et al., 2007). The optimal number of diffusion weighted directions is still unresolved and depends of different factors such as the robustness of the post processing algorithms, voxel size, available acquisition time and scan parameters (e.g., TE) (Tournier et al., 2012; Tournier et al., 2007).

DTT and DTI have been under explored for the evaluation of the pediatric spinal cord because of the relatively small size of the spinal cord and the motion artifacts induced by CSF pulsation, cardiac and respiration (Barakat et al., 2012; Saksena et al., 2016). However, development of newer pulse sequence methods such as reduced FOV has enabled reliable DTI collection and enabled further exploration of the spinal cord. The bulk physiologic motion about the cord, due to CSF pulsation, cardiac and respiration motion or due to swallowing hamper quality of diffusion weighted images. Some mitigation can be achievable with cardiac gating (Andre and Bammer, 2010). Cardiac gating was not used in this study. The lowest cervical levels, thoracic and thoracolumbar are the most sensitive to cardiac motion. Therefore, some cardiac related artifacts may have biased DTI and DTT measures. While this may be considered a limitation in this study, it is important to note that gating increases acquisition time and does not completely prevent subject motion. However, the absence of triggering might be linked to the relatively poor WM/GM contrast on the DTI data. Keeping the acquisition time relatively short was the priority for imaging in the pediatric population. This limitation could be overcome in the future by imaging the spinal cord using parallel or multiband DTI techniques, which will allow faster imaging.

8. Conclusion

DTI and DTT have proven to be effective techniques in the investigation and quantification of neurological development of the brain in pediatric subjects. However, few imaging studies have been conducted on the maturation of the pediatric spinal cord. In this study, these diffusion and fiber tracking techniques were successfully utilized to detect significant age-related changes of the spinal cord. This normative data and analysis could potentially help facilitate a more thorough understanding of the maturation process in pediatrics and serve as a basis for the detection of abnormal spinal conditions.

Acknowledgements

This work was supported by National Institute of Neurological Disorders of the National Institutes of Health under award number R01NS079635.

References

Alizadeh, M., Intintolo, A., Middleton, D.M., Conklin, C.J., Faro, S.H., Mulcahey, M.J., Mohamed, F.B., 2017. Reduced FOV diffusion tensor MR imaging and fiber tractography of the pediatric cervical spinal cord. Spinal Cord 55 (3), 314–320.

Andre, J.B., Bammer, R., 2010. Advanced diffusion-weighted magnetic resonance imaging techniques of the human spinal cord. Top. Magn. Reson. Imaging 21 (6), 367–378.

Barakat, N., Mohamed, F.B., Hunter, L.N., Shah, P., Faro, S.H., Samdani, A.F., Finsterbusch, J., Betz, R., Gaughan, J., Mulcahey, M.J., 2012. Diffusion tensor imaging of the normal pediatric spinal cord using an inner field of view echo planar imaging sequence. AJNR Am. J. Neuroradiol. 33 (6), 1127–1133.

Beaulieu, C., 2002. The basis of anisotropic water diffusion in the nervous system - a technical review. NMR Biomed. 15, 435–455.

Berman, J.I., Lanza, M.R., Blaskey, L., Edgar, J.C., Roberts, T.P., 2013. High angular resolution diffusion imaging (HARDI) probabilistic tractography of the auditory radiation. AJNR Am. J. Neuroradiol. 34 (8), 1573–1578.

Cancelliere, A., Mangano, F.T., Air, E.L., Jones, B.V., Altaye, M., Rajagopal, A., Holland, S.K., Hertzler, D.A., Yuan, W., 2013. DTI Values in Key White Matter Tracts From Infancy Through Adolescence. 34(7). pp. 1443–1449.

Chan, T.Y., Li, X., Mak, K.C., Cheung, J.P., Luk, K.D., Hu, Y., 2015 Dec. Normal values of cervical spinal cord diffusion tensor in young and middle-aged healthy Chinese. Eur. Spine J. 24 (12), 2991–2998.

Chang, L.C., Jones, D.K., Pierpaoli, C., 2005. RESTORE: robust estimation of tensors by outlier rejection. Magn. Reson. Med. 53 (5), 1088–1095.

Chang, Y., Jung, T.D., Yoo, D.S., Hyun, J.K., 2010. Diffusion tensor imaging and Fiber Tractography of patients with cervical spinal cord injury. J. Neurotrauma 27 (11), 2033–2040.

Conklin, C.J., Middleton, D.M., Alizadeh, M., Finsterbusch, J., Raunig, D.L., Faro, S.H., Shah, P., Krisa, L., Sinko, R., Delalic, J.Z., Mulcahey, M.J., Mohamed, F.B., 2016. Spatially selective 2D RF inner field of view (iFOV) diffusion kurtosis imaging (DKI) of the pediatric spinal cord. NeuroImage Clin. 11, 61–67.

DeVivo, M.J., Vogel, L.C., 2004. Epidemiology of spinal cord injury in children and adolescents. J. Spinal Cord Med. 27 (Suppl. 1), S4–10.

Facon, D., Ozanne, A., Fillard, P., Lepeintre, J., Tournoux-Facon, C., Ducreux, D., 2005. MR diffusion tensor imaging and fiber tracking in spinal cord compression. AJNR Am. J. Neuroradiol. 26, 1587.

Figley, C.R., Stroman, P.W., 2007. Investigation of human cervical and upper thoracic spinal cord motion: implications for imaging spinal cord structure and function. Magn. Reson. Med. 58 (1), 185–189.

Finsterbusch, J., 2012. Improving the performance of diffusion-weighted inner field-of-view echo-planar imaging based on 2D-selective radiofrequency excitations by tilting the excitation plane. J. Magn. Reson. Imaging 35, 984–992.

Giedd, J.N., Blumenthal, J., Jeffries, N.O., Castellanos, F.X., Liu, H., Zijdenbos, A., Paus, T., Evans, A.C., Rapoport, J.L., 1999. Brain development during childhood and adolescence: a longitudinal MRI study. Nat. Neurosci. 2 (10), 861–863.

Giorgio, A., Watkins, K.E., Douaud, G., James, A.C., James, S., De Stefano, N., Matthews, P.M., Smith, S.M., Johansen-Berg, H., 2008. Changes in white matter microstructure during adolescence. NeuroImage 39 (1), 52–61.

Giorgio, A., Watkins, K.E., Chadwick, M., James, S., Winmill, L., Douaud, G., De Stefano, N., Matthews, P.M., Smith, S.M., Johansen-Berg, H., James, A.C., 2010. Longitudinal changes in grey and white matter during adolescence. NeuroImage 49 (1), 94–103.

Good, C.D., Johnsrude, I.S., Ashburner, J., Henson, R.N., Friston, K.J., Frackowiak, R.S., 2001. A voxel-based morphometric study of ageing in 465 normal adult human brains. NeuroImage 14 (1 Pt 1), 21–36 Jul.

Goto, N., Otsuka, N., 1997. Development and anatomy of the spinal cord. Neuropathology 17, 25–31.

Helen, C.L., Christianne, L., Brian, B.L., Jacquie, H., Adam, K., Luis, E.B., Walter, H., Elisabeth, S., August 2014. Reliability and variability of diffusion tensor imaging (DTI) tractography in pediatric epilepsy. In: Epilepsy & Behavior. Vol. 37. pp.

116–122 ISSN 1525-5050.
Hüppi, P.S., Dubois, J., 2006. Diffusion tensor imaging of brain development. Semin. Fetal Neonatal Med. 11 (6), 489–497.
Iannetti, P., Nicita, F., Spalice, A., Parisi, P., Papetti, L., Verrotti, A., 2011. Fiber tractography assessment in double cortex syndrome. Childs Nerv. Syst. 27 (8), 1197–1202.
Izbudak, I., Dumrongpisutikul, N., Thompson, C.B., Tekes, A., Thurnher, M., Huisman, T.A., 2015. Diffusion tensor scalars vary with age and across spinal levels in children. J. Neurol. 6 (4), 1–6.
Kanehiro, F., Tsunehiko, K., Masayuki, Y., Keigo, H., Osahiko, T., Yuji, K., Suketaka, M., Yoshiaki, T., Masaya, N., 2013. Diffusion tensor imaging and tractography of the spinal cord: from experimental studies to clinical application. Exp. Neurol. 242, 74–82.
Knosche, T.R., Anwander, A., Liptrot, M., Dyrby, T.B., 2015. Validation of tractography: comparison with manganese tracing. Hum. Brain Mapp. 36 (10), 4116–4134.
Ko, H.Y., Park, J.H., Shin, Y.B., Baek, S.Y., 2004. Gross quantitative measurements of spinal cord segments in human. Spinal Cord 42 (1), 35–40.
Lassek, A.M., 1942. The human pyramidal tract v. Postnatal changes in the axons of the pyramids. Arch. Neurpsych. 47 (3), 422–427.
Lassek, A.M., Rasmussen, G.L., 1938. A quantitative study of the newborn and adult spinal cords of man. J. Comp. Neurol. 69, 371–379.
Lebel, C., Deoni, S., 2018. The development of brain white matter microstructure. NeuroImage 1–112 Jan 3.
Maier, S.E., Mamata, H., 2005. Diffusion tensor imaging of the spinal cord. Ann. N. Y. Acad. Sci. 1064, 50–60.
Middleton, D.M., Mohamed, F.B., Barakat, N., Hunter, L.N., Shellikeri, S., Finsterbusch, J., Faro, S.H., Shah, P., Samdani, A.F., Mulcahey, M.J., 2014. An investigation of motion correction algorithms for pediatric spinal cord DTI in healthy subjects and patients with spinal cord injury. Magn. Reson. Imaging 32 (5), 433–439.
Mohamed, F.B., Hunter, L.N., Barakat, N., Liu, C.S., Sair, H., Samdani, A.F., Betz, R.R., Faro, S.H., Gaughan, J., Mulcahey, M.J., 2011. Diffusion tensor imaging of the pediatric spinal cord at 1.5T: preliminary results. AJNR 32 (2), 339–345.
Mori, S., Van Zijl, P.C., 2002. Fiber tracking: principles and strategies – a technical review. NMR Biomed. 15 (7–8), 468–480.
Mulcahey, M.J., Samdani, A.F., Gaughan, J.P., Barakat, N., Faro, S., Shah, P., Betz, R.R., Mohamed, F.B., 2013. Diagnostic accuracy of diffusion tensor imaging for pediatric cervical spinal cord injury. Spinal Cord 51 (7), 532–537.
Paus, T., 2010 Feb. Growth of white matter in the adolescent brain: myelin or axon? Brain Cogn. 72 (1), 26–35.
Prados, F., Ashburner, J., Blaiotta, C., et al., 2017. Spinal cord grey matter segmentation challenge. NeuroImage 152, 312–329.
Renoux, J., Facon, D., Fillard, P., Huynh, I., Lasjaunias, P., Ducreux, D., 2006. MR diffusion tensor imaging and fiber tracking in inflammatory diseases of the spinal cord. AJNR Am. J. Neuroradiol. 27 (9), 1947–1951.
Saksena, S., Middleton, D.M., Krisa, L., Shah, P., Faro, S.H., Sinko, R., Gaughan, J., Finsterbusch, J., Mulcahey, M.J., Mohamed, F.B., 2016. Diffusion tensor imaging of the normal cervical and thoracic pediatric spinal cord. AJNR Am. J. Neuroradiol. 37 (11), 2150–2157.
Setzer, M., Murtagh, R.D., Murtagh, F.R., Eleraky, M., Jain, S., Marquardt, G., Seifert, V., Vrionis, F.D., 2010. Diffusion tensor imaging tractography in patients with intramedullary tumors: comparison with intraoperative findings and value for prediction of tumor resectability. J. Neurosurg. Spine 13 (3), 371–380.
Sherman, J.L., Nassaux, P.Y., Citrin, C.M., 1990. Measurements of the normal cervical spinal cord on MR imaging. AJNR Am. J. Neuroradiol. 11, 369–372.
Singhi, S., Tekes, A., Thurnher, M., Gilson, W.D., Izbudak, I., Thompson, C.B., Huisman, T.A., 2012. Diffusion tensor imaging of the maturing paediatric cervical spinal cord: from the neonate to the young adult. J. Neuroradiol. 39 (3), 142–148.
Stiles, J., Jernigan, T.L., 2010. The basics of brain development. Neuropsychol. Rev. 20 (4), 327–348.
Tournier, J.D., Calamante, F., Connelly, A., 2007. Robust determination of the fiber orientation distribution in diffusion MRI: non-negativity constrained super-resolved spherical deconvolution. NeuroImage 35, 1459–1472.
Tournier, J.D., Calamante, F., Connelly, A., 2012. MRtrix: diffusion tractography in crossing fiber regions. Int. J. Imaging Syst. Technol. 22, 53–66.
Vedantam, A., Jirjis, M.B., Schmit, B.D., Wang, M.C., Ulmer, J.L., Kurpad, S.N., 2013. Characterization and limitations of diffusion tensor imaging metrics in the cervical spinal cord in neurologically intact subjects. J. Magn. Reson. Imaging 38, 861–867.
Verhaart, W.J.C., 1950. Hypertrophy of pes pedunculi and pyramidal result of degeneration of contralateral corticofugal fiber tracts. J. Comp. Neurol. 92, 1–15.
Wang, K., Song, Q., Zhang, F., Chen, Z., Hou, C., Tang, Y., Chen, S., Hao, Q., Shen, H., 2014. Age-related changes of the diffusion tensor imaging parameters of the normal cervical spinal cord. Eur. J. Radiol. 83, 2196–2202.
Zhang, H., Schneider, T., Wheeler-Kingshott, C.A., Alexander, D.C., 2012. NODDI: practical in vivo neurite orientation dispersion and density imaging of the human brain. NeuroImage 61 (4), 1000–1016.